# Analytic versus CFD approach for kinetic modeling of gas phase photocatalysis

# Analytic *versus* CFD approach for kinetic modeling of gas phase photocatalysis

Sammy W. Verbruggen [a,b], Silvia Lenaerts [a], Siegfried Denys [a,*]

[a] Sustainable Energy and Air Purification, Department of Bioscience Engineering, University of Antwerp, Groenenborgerlaan 171, B-2020 Antwerp, Belgium.
* E-mail: Siegfried.Denys@uantwerp.be
Fax: +32 3 265 32 25. Tel: +32 3 265 32 30.

[b] Center for Surface Chemistry and Catalysis, KU Leuven, Kasteelpark Arenberg 23, B-3001 Heverlee (Leuven), Belgium

**Abstract**

In this work two methods for determining the Langmuir-Hinshelwood kinetic parameters for a slit-shaped flat bed photocatalytic reactor are compared: an analytic mass transfer based model adapted from literature and a Computational Fluid Dynamics (CFD) approach that was used in conjunction with a simplex optimization routine. Despite the differences between both approaches, similar values for the kinetic parameters and similar trends in terms of their UV intensity dependence were found. Using an effectiveness-*NTU* (Number of Transfer Units) approach, the analytic mass transfer based method could quantify the relative contributions of the rate limiting steps through a reaction effectiveness parameter. The numeric CFD approach on the other hand could yield the two kinetic parameters that determine the photocatalytic reaction rate simultaneously. Furthermore, it proved to be more accurate as it accounts for the spatial variation of flow rate, reaction rate and concentrations at the surface of the photocatalyst. We elaborate this dual kinetic analysis with regard to the photocatalytic degradation of acetaldehyde in air over a silicon wafer coated with a layer of $TiO_2$ P25 (Evonik) and study the usefulness and limitations of both strategies.

**Keywords**

Photocatalysis; kinetics; mass transfer; gas phase; computational fluid dynamics (CFD); acetaldehyde

## 1. Introduction

Among the advanced oxidation processes (AOPs) for removal of volatile organic compounds (VOCs) from air, photocatalytic oxidation (PCO) of pollutants is considered a very promising technology [1, 2]. In contrast to filters, PCO can achieve complete mineralization of harmful VOCs to $CO_2$ and $H_2O$ using only light as the energy source [3]. Commonly used photocatalysts are transition metal oxides, with $TiO_2$ most often the photocatalyst of choice since it is relatively inexpensive, non-toxic, chemically stable and it has relatively high reactivity for elimination of airborne pollutants under UV irradiation [4]. Recently, the integration of $TiO_2$ photocatalysis for air purification in heating, ventilation and air conditioning (HVAC) systems was investigated at several research groups and summarized in various excellent review articles [5-7]. As $TiO_2$ photocatalysis is operated at ambient conditions, it is well suited for integration in (existing) HVAC equipment.

One of the main challenges when studying the potential of PCO reactors for HVAC applications is to find appropriate kinetic models and kinetic parameters that accurately describe the rate of decontamination by photocatalytic coatings under a range of operating conditions. Obviously, one must be adept at understanding and describing the fundamental principles of mass transfer (diffusion, adsorption-desorption) and reaction kinetics that occur simultaneously. Defining and describing pollutant transport in reactors, the interactions of pollutants with the catalytic surface and irradiation phenomena is a complex matter. Mass transfer based models for the determination of kinetic parameters were developed by several researchers [8, 9]. A mechanistic method to understand the interacting effects of reaction area, mass transfer, kinetic reaction rate and other influencing factors was developed by Zhang *et al* [10]. Their method is based on two parameters, the 'number of mass transfer units' *NTU*, and the fractional conversion, $\varepsilon$, for describing the performance of PCO reactors. The method was later improved by the authors, allowing for variable rate coefficients and variable mass transfer coefficients along the flow direction in the PCO reactor [11] and in the perimetric direction [12]. In the improved models three parameters were defined: the 'ideal reaction number of mass transfer units' $NTU_{ideal}$, the ideal fractional conversion, $\varepsilon_{ideal}$, and the reaction effectiveness, $\eta$.

As we will show, analytic mass transfer based methods as the one described above can yield an adequate estimation of the kinetic parameters. However, a large drawback of such methods is the requirement of a substantial set of experimental data in order to curve-fit measured reaction rates and pollutant concentrations using a given kinetic expression. Furthermore, the pollutant concentrations used in these models should be the concentrations in the immediate vicinity of the reaction surface. Obviously, these concentrations are difficult to measure directly. Depending on where the concentration is measured and the geometry of the PCO reactor used (flat plate, annular, honeycomb, packed-bed, …) errors are expected, limiting the applicability of the obtained kinetic parameters.

In this work we will therefore compare the above described analytical mass transfer based method for the determination of kinetic parameters, with a numeric approach using computational fluid dynamics (CFD). CFD is an approach based on numeric solutions of the governing equations for fluid motion, heat transfer and species transport [13]. Today, CFD can handle sophisticated modularity and is able to couple different prevalent physicochemical mechanisms by solving numeric algorithms [14]. In the context of developing PCO reactors for HVAC systems, CFD is useful for determining the

kinetic parameters based on experiments conducted in a photocatalytic test reactor on one side and on the other side it is useful as a design, characterization and development tool for upscaling reactors towards the application scale [15-19]. CFD is the designated approach for determining location-dependent pollutant concentrations (even near the catalyst surface), as it considers the actual geometrical design of the reactor and all characteristics of the airflow. Furthermore, as will be demonstrated one single measurement can be used to simultaneously extract several relevant parameters. Using an optimization procedure, we will demonstrate how this numeric multiphysics approach is even more powerful in accurately determining kinetic parameters than the previously established mass transfer based models.

## 2. Material and methods

### *2.1. Photocatalytic reactor and degradation test*

The photoreactor used in this work is a continuous flow, single pass, slit-shaped flat bed photoreactor (Fig. 1) as described in previous work [20, 21]. The reactor is constructed in stainless steel and sealed from the top by a 4 mm quartz plate. A sealing rubber is sandwiched between both halves of the reactor, resulting in a reactor slit height of 2.5 mm and width of 20 mm. A Philips Cleo (25 W) UVA light bulb was placed 2, 4 or 6 cm above the samples, resulting in an incident intensity on the photocatalytic surface of (2.6 ± 0.1), (1.6 ± 0.1) and (1.3 ± 0.1) mW $cm^{-2}$ respectively, as measured by a calibrated intensity meter (Avantes Avaspec-3648).

Acetaldehyde was used as model compound for indoor air contamination [22]. Acetaldehyde (Air Liquide, 1% in $N_2$) was mixed with clean air (Air Liquide Alphagaz) using mass flow controllers and dosed to the reactor set-up at an inlet concentration of approximately 22, 43 or 53 ppmv at an effective total gas flow rate of 300, 375, 450, 525 or 600 $cm^3$ $min^{-1}$. This way, 15 different reaction conditions were tested for each of the three incident UV intensities. As described in earlier work, the concentrations of acetaldehyde and $CO_2$ were monitored on-line at the reactor outlet by FTIR spectroscopy using the IR peaks at 2728 $cm^{-1}$, corresponding to the C-H stretch of acetaldehyde $\nu$(C-H) and at 2360 $cm^{-1}$, corresponding to the asymmetric $CO_2$ stretch $\nu_{as}(CO_2)$ [23, 24]. In all our experiments the relative humidity of the gas stream was kept at 5%, by leading part of the clean airflow through a gas wash bottle. In our previous work this has been established as an appropriate amount of moisture for obtaining reliable and reproducible measurements using the present reactor configuration [20, 21]. The catalyst used in our study was $TiO_2$ Aeroxide P25 (Evonik). The catalyst was suspended in ethanol, ultrasonically stirred, spin coated on cleaned silicon wafers and dried at 363 K. The test sample (15 mm by 60 mm) was placed near the center of the reactor slit.

### *2.2. Reaction Kinetics*

In our earlier work we have clearly observed (and quantified) adsorption of acetaldehyde on a $TiO_2$ surface [24]. We therefore assume the PCO reaction to obey Langmuir-Hinshelwood (LH) kinetics. It should be emphasized that the LH mechanism should be thought of as an ideal, empirical limit. Other mechanisms have been proposed and studied as well. One could consider all detailed mechanistic steps, including the intermediates and by-products formed during the actual PCO and obtain very complex rate expressions [25]. Assuming simple Langmuir behavior (monolayer coverage, uniform surface, all adsorption sites are equivalent, and no interaction between adsorbates), the fractional coverage of acetaldehyde on an illuminated $TiO_2$ surface is given by the well-known expression (eq. 1):

$$\theta = \frac{K_L C_{VOC}}{1 + K_L C_{VOC}} \qquad \text{(eq. 1)}$$

where $K_L$ is the Langmuir adsorption constant under illumination [$m^3$ $mol^{-1}$] (equivalent to $k_{adsorption}/k_{desorption}$) and $C_{VOC}$ the acetaldehyde concentration [mol $m^{-3}$]. Considering the abundant amount of oxygen in indoor air, the fractional coverage of oxygen is usually close to unity and the reaction rate for PCO reactions is commonly written as the unimolecular type LH mechanism given by (eq. 2):

$$r = k_{LH}\theta_{VOC} = \frac{k_{LH} K_L C_{VOC}}{1 + K_L C_{VOC}} = k_{\text{app}} C_{VOC} \qquad \text{(eq. 2)}$$

where $k_{LH}$ [mol $m^{-2}$ $s^{-1}$] is the Langmuir-Hinshelwood rate coefficient and $k_{app}$ [m $s^{-1}$] is the apparent reaction rate coefficient. From the next section it will be clear that $k_{app}$ should be regarded as a local parameter $k_{app}(x)$ that is dependent on the VOC concentration in the air adjacent to the reaction surface, the incident light intensity, etc. [11]. Throughout our analysis $C_{VOC}$ should therefore be regarded as the VOC concentration in close proximity of the catalyst surface. It is different from the bulk VOC concentration in the airflow, further down denoted as $C_{VOC,\infty}$. In practice the active phase is not evenly distributed over the surface. The dispersion depends on the particular support structure and the method used for coating the support structure with the active phase [26]. As a consequence of the complexity, obtaining straightforward and universally valid kinetic parameters for all conditions is an infeasible intent, and parameters should be considered in relation to a specific set of operating conditions.

Being an essential component of PCO reactions, UV light wavelength and intensity should be somehow accounted for in the kinetic model. In general, it was observed that UV intensity has a first-order effect on the reaction rate at low intensities (electron-hole pairs are consumed more rapidly by chemical reactions than by recombination), and a half-order effect at higher intensities (suggesting that recombination of electron-hole pairs dominates consumption by the PCO reaction) [27]. The following equation (eq. 3) is generally used to account for UV light intensity:

$$r = r_e \left( \frac{I}{I_e} \right)^n \qquad \text{(eq. 3)}$$

Where $I$ is the UV intensity, $I_e$ is the UV intensity for which the reaction rate, $r_e$, has been evaluated and $n$ is between 1 and 0,5 depending on the UV intensity.

### *2.3. Mass transfer based model*

#### *2.3.1. Model outline*

VOC removal by PCO is a heterogeneous surface process that can best be described as a combined effect of VOC diffusion through the reactor, VOC transfer to and from the reaction surface (adsorption-desorption equilibrium) and VOC decomposition at the catalyst surface. As a result, both the mass transfer rate and the reaction rate can be limiting parameters. In order to yield kinetic parameters that are useful for designing, developing and upscaling PCO reactors, the mass transfer of the species involved in the reactions should therefore be accounted for. The mass transfer model used in the present work is based on the analysis followed by Yang *et al.* [11], adapted for the geometry of the slit-shaped reactor in our work (Fig. 2).

With the notations of the figure, the mass conservation equation for an infinitely small section of the reactor can be written as (eq. 4):

$$G\frac{\partial C_{VOC,\infty}(x)}{\partial x}dx = -j(x)\,p\,dx \qquad \text{(eq. 4)}$$

where $x$ is the coordinate in the flow direction, $G$ [$m^3\ s^{-1}$] is the volumetric airflow rate, $C_{VOC,\infty}(x)$ [$mol\ m^{-3}$] is the VOC concentration in the bulk of the airflow and $p$ [m] is the length of the reaction surface perpendicular to the flow direction. The mass transfer rate at the catalyst surface, $j(x)$, expressed per unit reaction surface area, is given by (eq. 2). As mentioned above, the pollutant concentration used in this expression should be the concentration at the reaction surface, which is related to the bulk concentration $C_{VOC,\infty}$ in the airflow by the general expression for mass convection at the boundary surface (eq. 5):

$$j(x) = k_{app}(x)C_{VOC}(x) = h_{mass}(x)\left[C_{VOC,\infty}(x) - C_{VOC}(x)\right]$$
$$or \quad j(x) = \frac{C_{VOC,\infty}(x)}{1/h_{mass}(x) + 1/k_{app}(x)} \qquad \text{(eq. 5)}$$

where $h_{mass}(x)$ [$m\ s^{-1}$] is the local convective mass transfer coefficient. Following the analysis of Yang *et al.* [11], the mass conservation equation for the infinitely small section of the reactor space above the catalyst surface (Fig. 2) then becomes (eq. 6):

$$G\frac{\partial C_{VOC,\infty}(x)}{\partial x}dx = -K_t(x)C_{VOC,\infty}(x)\,p\,dx \qquad \text{(eq. 6)}$$

Where $K_t(x) = \dfrac{1}{1/h_{mass}(x) + 1/k_{app}(x)}$ is the local 'total removing factor'.

Solving (eq. 6) to yield the VOC removal over the entire length $L$ of the active surface gives (eq. 7):

$$C_{VOC,\infty,out} = C_{VOC,\infty,in}e^{-K_t A/G} \qquad \text{(eq. 7)}$$

where $K_t = \int_0^L K_t(x)dx \Big/ L$ is the average total removing factor over the length of the active surface and $A$ is the entire surface of the catalyst. Notice that the average total removing factor combines the average convective mass transfer coefficient $h_{mass}$ and the average apparent reaction rate coefficient $k_{app}$ (eq. 8):

$$K_t = \frac{1}{1/h_{mass} + 1/k_{app}} \quad \text{(eq. 8)}$$

At this point in their analysis, Yang *et al.* [11] found an analogy with the effectiveness-*NTU* (the number of transfer units) method generally used for heat exchangers [28], and they developed a very elegant approach which greatly simplifies the evaluation of the VOC removal performance of PCO reactors. Whereas the *NTU* approach for heat exchangers defines the effectiveness of a heat exchanger in terms of the maximum possible heat transfer that can be hypothetically achieved in a heat exchanger of infinite length, the $NTU_{PCO}$ method as suggested by Yang *et al.* [11] reasons from an 'ideal' PCO reactor were $k_{app}$ approaches infinity and the PCO reaction is controlled by mass transfer only. In analogy with heat exchangers, the number of mass transfer units for a PCO reactor may be defined as (eq. 9):

$$NTU_{PCO} = \frac{K_t A}{G} \quad \text{(eq. 9)}$$

and the VOC removal efficiency of the PCO reactor can be represented by the fractional conversion, $\varepsilon$ (eq. 10):

$$\varepsilon = \frac{C_{VOC,\infty,in} - C_{VOC,\infty,out}}{C_{VOC,\infty,in}} = 1 - e^{-NTU_{PCO}} \quad \text{(eq. 10)}$$

For an ideal system $k_{app}$ approaches infinity. In such case the PCO reaction is controlled by mass transfer only (eq. 11):

$$\varepsilon_{ideal} = 1 - e^{-NTU_{PCO,ideal}} \quad \text{with} \quad NTU_{PCO,ideal} = \frac{h_{mass} A}{G} \quad \text{(eq. 11)}$$

where $\varepsilon_{ideal}$ is the fractional conversion for the hypothetically ideal PCO reactor (with highest PCO activity) and $h_{mass} = \int_0^L h_{mass}(x)dx \Big/ L$ is the average convective mass transfer coefficient over the length of the active surface. The relative contributions of mass transfer and the activity of the photocatalyst can then be expressed by the reaction effectiveness, $\eta$, defined as (eq. 12):

$$\eta = \frac{\varepsilon}{\varepsilon_{ideal}} \quad \text{(eq. 12)}$$

Therefore, PCO reactions with $\eta$ approaching unity are controlled by mass transfer, whereas processes with $\eta$ approaching zero are under kinetic control.

### *2.3.2. General strategy*

From the previous analysis, a general strategy may be formulated in order to determine the kinetic parameters $k_{LH}$ and $K_L$ from a given set of experiments:

1. Calculate the Reynolds number, *Re*, based on the experimental conditions and reactor geometry

2. Calculate the (local) Sherwood number, *Sh(x)* using tabulated empirical expressions and from this determine $h_{mass}(x)$ using (eq. 13):

$$Sh(x) = \frac{h_{mass}(x) D_h}{D} \quad \text{(eq. 13)}$$

with $D_h$ [m] the hydraulic diameter and $D$ [$m^2$ $s^{-1}$] the diffusion coefficient of the VOC in air.

3. Calculate $NTU_{PCO,ideal}$ and $\varepsilon_{ideal}$ (eq. 11)

4. Determine the reaction effectiveness $\eta$ (eq. 12), with $\varepsilon$ determined experimentally

5. From $\varepsilon$, $NTU_{PCO}$ can be calculated (eq. 10)

6. Determine the average total removing factor $K_t$ from the definition of $NTU_{PCO}$ (eq. 9)

7. Calculate the average apparent reaction rate coefficient $k_{app}$ from $K_t$ (eq. 8)

8. Calculate $C_{VOC}$ from the equality in (eq. 5), which gives (in average terms)

$$C_{VOC} = \frac{C_{VOC,\infty}}{1 + k_{app}/h_{mass}} = \frac{C_{VOC,\infty,in} + C_{VOC,\infty,out}}{2\left(1 + k_{app}/h_{mass}\right)} \quad \text{(eq. 14)}$$

It should be mentioned here that both $C_{VOC}$ and $C_{VOC,\infty}$ vary over the length of the reaction surface. In the analytic analysis followed here, an average value for $C_{VOC}$ is determined from the inlet and outlet bulk concentrations.

9. Plot $1/k_{app}$ versus $C_{VOC}$ for all different experimental conditions. From the observed linear fit, $k_{LH}$ can be derived as the inverse slope and $K_L$ can be subsequently calculated from the intercept with the Y-axis, $k_{LH}^{-1}K_L^{-1}$ ((eq. 2) reorganized).

### *2.4. Numeric approach (CFD)*

CFD simulations were carried out using Comsol 4.3b. The CFD geometry of the photoreactor and an impression of the computational grid are shown in Fig. 3. The computational grid consisted of approximately 250,000 tetrahedral cells with refinement at the boundaries, inlet and outlet of the reactor. Grid dependency and mesh quality were ensured.

Considering the low Reynolds numbers (see below), a laminar flow model was used. Convection and diffusion of acetaldehyde was accounted for by the scalar transport equation (eq. 15):

$$\nabla \cdot \left(-D \nabla C_{VOC,\infty}\right) + \mathbf{u} \cdot \nabla C_{VOC,\infty} = 0 \quad \text{(eq. 15)}$$

with **u** being the velocity vector of the air [m $s^{-1}$]. The photocatalytic reaction was included as an outward flux $r_{LH}$ [mol $m^{-2}$ $s^{-1}$] on the active surface, expressed in terms of the LH reaction kinetic parameters (eq. 16):

$$r_{LH} = -\frac{k_{LH} K_L C_{VOC}}{1 + K_L C_{VOC}} \quad \text{(eq. 16)}$$

Notice that in the CFD calculations, $C_{VOC}$ is in effect the acetaldehyde concentration calculated for the flow near the active surface. This is an anisotropic variable as it typically varies spatially over the surface. This degree of spatial accuracy cannot be accounted for by the mass transfer based model.

Using the appropriate experimental inlet concentrations and total gas flow rates at the reactor inlet, stationary solutions were generated and the surface averaged concentration of acetaldehyde at the outlet surface, $C_{VOC,\infty,CFD}$, was compared to the experimentally obtained value $C_{VOC,\infty,exp}$.

for determining the kinetic parameters, a Comsol optimization module was used in conjunction with the CFD calculations. Hereby, for each experimental condition an objective function was defined as (eq. 17):

$$Obj = \left| C_{VOC,\infty,out,exp} - C_{VOC,\infty,out,CFD} \right| \quad \text{(eq. 17)}$$

A simplex optimization routine (the Nelder-Mead method) was used for finding the local minimum of this objective function by changing the kinetic parameters within certain constraints. For two variables $k_{LH}$ and $K_L$, this method is a pattern search that compares the objective function values at the three vertices of a triangle. The worst vertex, where Obj($k_{LH}$, $K_L$) is largest, is rejected and replaced with a new vertex. A new triangle is formed and the search is continued. The process generates a sequence of triangles for which the objective function values at the vertices get smaller and smaller. The size of the triangles is reduced and the coordinates ($k_{LH}$, $K_L$) of the minimum point are found for this particular experimental condition. This strategy is then repeated for all other experimental conditions involved. The obtained values are eventually averaged and reported.

## 3. Results and discussion

### *3.1 Analytic solution: mass transfer based model*

The general parameters related to reactor geometry and fluid properties are listed in Table 1 for completeness. In the following we will report intermediate results of our analysis on the experiments conducted under illumination at the intermediate intensity of (1.6 ± 0.1) mW cm$^{-2}$. The results for the highest and lowest intensities are obtained in a similar way and will be summarized at the end. For the five different flow rates, all relevant parameters to be used in, or obtained from the analytic mass transfer based model are given in Table 2.

It can be observed that under all conditions the Reynolds numbers are low (between 29 and 59), meaning the reactor is operated in a laminar flow regime at all times. An important implication of this laminar flow condition is that the Sherwood number becomes independent of the volumetric flow rate [28]. Consequently the mass transfer coefficient, $h_{mass}$ can be considered constant for all experimental conditions (eq. 13). Evidently, the fractional conversion $\varepsilon$ decreases as the volumetric flow rate or the inlet concentration increases. The reactor is operated in a regime in which the maximal attainable conversion $\varepsilon_{ideal}$ also drops with increasing flow rate. The reaction effectiveness $\eta$ lies between 0.10 and 0.53, indicating that under the present conditions there is a significant contribution of both mass transfer as well as kinetic phenomena. This also applies for the higher and lower illumination intensities ($\eta$ in the range 0.27-0.79 and 0.07-0.31, respectively). The observed trends in $\eta$ reflect the dominant character of mass transfer on the overall removal efficiency in the case of high UV intensity, low flow rates (i.e. large contact time) and low inlet concentrations, whereas the photocatalytic reaction is rather kinetically controlled for low intensities, high flow rates and high concentrations.

As discussed above, the kinetic parameters $k_{LH}$ and $K_L$ can be derived from the slope and intercept of the plot of the reciprocal of $k_{app}$ *versus* the average surface concentration $C_{VOC}$ (eq. 15). The $k_{app}^{-1}$ *versus* $C_{VOC}$ plots for all three illumination intensities are presented in Fig. 4 and the extracted mass transfer based kinetic parameters are listed in Table 3. First of all it is good to note that for all intensities $k_{app}^{-1}$ *versus* $C_{VOC}$ can indeed be well fitted linearly ($R^2$ values between 0.97-0.99). In

addition the plots demonstrate that our experimental conditions cover a very wide range of reaction effectiveness values (min. 0.07, max. 0.79). As mentioned with respect to Table 2 above, low values of $\eta$ are observed in the case of low incident intensity and indicate a photocatalytic reaction that is mainly under kinetic control (Fig. 4a). The opposite is true for the high incident intensity experiments, characterized by larger values for $\eta$ (Fig. 4c). From Table 3 it can be seen that the LH reaction constant increases with increasing intensity. This has been discussed in literature for regimes that are (at least in part) under kinetic control [29]. Applying (eq. 3) results in a first order (n = 1, $R^2$ = 0.997) correlation between the overall reaction rate *r* (last column in Table 3) and the intensity. The Langmuir adsorption constant under illumination, $K_L$, decreases with increasing intensity, which is in accordance with previous observations [30, 31]. It is good to realize that the Langmuir adsorption coefficient determined under illumination can be quite different from the one obtained for adsorption in dark.

### *3.2. Numeric solution: CFD method with optimization procedure*

Some typical CFD results are shown in Fig. 5. The figure shows the distributions of acetaldehyde concentration through the photoreactor at steady state conditions for simulations at the intermediate UV intensity of (1.6 ± 0.1) mW $cm^{-2}$. All distributions shown in the figure resulted from the same acetaldehyde inlet concentration of 43 ppmv (or 0.00179 mol $m^{-3}$), while the total inlet gas flow rate ranged from 300 $cm^3$ $min^{-1}$ to 600 $cm^3$ $min^{-1}$. For these simulations, the kinetic parameters calculated in accordance with the mass transfer based analytic method (Table 3) were used. Similar results were obtained at higher and lower UV intensity. The results clearly show the effect of the flow rate on the distribution of acetaldehyde. At higher flow rates, the contact time at the photoactive surface becomes shorter, resulting in a lower overall removal efficiency in the reactor. The CFD simulations clearly illustrate the typical spatial variation of $C_{VOC}$ at the photoreactor surface, which is not taken into account in the analytic mass transfer based approach. Besides, the outlet concentrations in the case of the CFD simulations were evaluated as the surface averaged concentration of acetaldehyde at the outlet surface of the reactor geometry. This corresponds to the experimental procedure where concentrations are evaluated in the photoreactor outlet gas stream. Interestingly, this concentration may differ from the VOC concentration at the end of the photoactive surface (the 'outlet concentration' considered by the analytic mass transfer model), as some mixing occurs at the geometry region between the active surface and the outlet section. This is clear from the acetaldehyde concentration distributions.

Using the Nelder-Mead simplex optimization routine, the kinetic parameters were derived for each of the 15 independent simulations of the 15 reaction conditions that were tested for each of the three incident UV intensities. The resulting individually optimized values for $k_{LH}$ and $K_L$ enabled to numerically replicate the experimentally determined outlet concentrations with deviations typically smaller than 0.03%. The average values for $k_{LH}$ and $K_L$ over the entire set of experiments, are listed in Table 3 for the three incident UV intensities. In order to gain confidence in the optimization procedure, the constraint intervals within which the optimization pattern search was started, were chosen sufficiently large so as to avoid local 'false' minima of the objective function. From Table 3 it can be seen that the optimized LH kinetic parameters show the same trends as the ones obtained using the analytic mass transfer based approach, i.e. a reaction constant with a distinct UV intensity proportionality and a constant Langmuir adsorption constant for the lower intensities. The optimized values for $k_{LH}$ and $K_L$ are about 15 to 20% higher than the corresponding parameters obtained from

the analytic approach. This can be ascribed to the aforementioned mixing of air that has passed directly over the catalytic surface (and thus has a lower VOC concentration) with bypassed and thus untreated air carrying a higher VOC concentration. In order to compensate for this mixing effect, the reaction rate predicted by the optimization routine must be higher. The analytic approach does not account for this phenomenon.

To illustrate the improvement in accuracy when determining the kinetic parameters using the CFD optimization approach, Fig. 6 presents a comparison of both methods. The figure shows calculated outlet VOC concentrations *versus* experimentally determined concentrations for both methods, for each of the 15 reaction conditions. For the analytic mass transfer method, outlet VOC concentrations were calculated from (eq. 7), using the mass transfer based kinetic parameters from Table 3 and the appropriate VOC inlet concentrations and flow rates applied in the experiments. For the CFD approach, the average numeric kinetic parameters from Table 3 were used. The results clearly demonstrate the improvement of the CFD approach in accurately determining the kinetic parameters.

## 4. Conclusion

We have applied and studied two methodologies for determining the kinetic parameters of a slit-shaped flat bed photocatalytic reactor. The first is an analytic approach based on a mass transfer model combined with Langmuir Hinshelwood reaction kinetics. The second approach is a numeric method based on Computational Fluid Dynamics. It is good to realize that the analytic mass transfer based method, as well as the numeric CFD method both have their merits. The effectiveness-*NTU* approach of the mass transfer model yields specific information on the nature of rate limiting behavior through the reaction effectiveness parameter $\eta$. The numeric CFD method does not explicitly distinguish between mass transfer and kinetic control. The main strength of the CFD method lies in its feasibility of accurately calculating the spatial variation of flow rate, reaction rate and concentrations at the reactive surface, which is not accounted for by the analytic mass transfer based approach. Besides, the mass transfer approach requires a substantial dataset in order to derive one single value for both kinetic parameters $k_{LH}$ and $K_L$, whereas the numeric CFD approach can yield good estimates for several parameters simultaneously from one experiment. Furthermore we have demonstrated that using an optimization procedure precise values for the kinetic parameters are obtained and experimentally obtained data can be accurately simulated or predicted. The CFD approach is therefore well suited for the design of alternative reactor geometries once a good estimation of the kinetic parameters is known.

## Acknowledgements

S.W.V. acknowledges the Research Foundation of Flanders (FWO) for financial support.

## References

[1] A. Di Paola, E. Garcia-Lopez, G. Marci, L. Palmisano, A survey of photocatalytic materials for environmental remediation, J. Hazard. Mater. 211 (2012) 3-29.

[2] K. Demeestere, J. Dewulf, H. Van Langenhove, Heterogeneous photocatalysis as an advanced oxidation process for the abatement of chlorinated, monocyclic aromatic and sulfurous volatile organic compounds in air: State of the art, Crit. Rev. Env. Sci. Technol. 37 (2007) 489-538.

[3] O. Carp, C.L. Huisman, A. Reller, Photoinduced reactivity of titanium dioxide, Prog. Solid State Chem. 32 (2004) 33-177.

[4] T. Ochiai, A. Fujishima, Photoelectrochemical properties of TiO2 photocatalyst and its applications for environmental purification, J. Photochem. Photobiol., *C* 13 (2012) 247-262.

[5] J. Mo, Y. Zhang, Q. Xu, J.J. Lamson, R. Zhao, Photocatalytic purification of volatile organic compounds in indoor air: A literature review, Atmos. Environ. 43 (2009) 2229-2246.

[6] Y. Paz, Application of TiO2 photocatalysis for air treatment: Patents' overview, Appl. Catal., B 99 (2010) 448-460.

[7] J. Zhao, X. Yang, Photocatalytic oxidation for indoor air purification: a literature review, Build. Environ. 38 (2003) 645-654.

[8] R.J. Hall, P. Bendfeldt, T.N. Obee, J.J. Sangiovanni, Computational and experimental studies of UV/titania photocatalytic oxidation of VOCs in honeycomb monoliths, J. Adv. Oxid. Technol. 3 (1998) 243-252.

[9] M.M. Hossain, G.B. Raupp, S.O. Hay, T.N. Obee, Three-dimensional developing flow model for photocatalytic monolith reactors, AIChE J. 45 (1999) 1309-1321.

[10] Y. Zhang, R. Yang, R. Zhao, A model for analyzing the performance of photocatalytic air cleaner in removing volatile organic compounds, Atmos. Environ. 37 (2003) 3395-3399.

[11] R. Yang, Y.P. Zhang, R.Y. Zhao, An improved model for analyzing the performance of photocatalytic oxidation reactors in removing volatile organic compounds and its application, J. Air Waste Manage. Assoc. 54 (2004) 1516-1524.

[12] J. Mo, Y. Zhang, R. Yang, Novel insight into VOC removal performance of photocatalytic oxidation reactors, Indoor air 15 (2005) 291-300.

[13] J.D. Anderson, Computational Fluid Dynamics. The basics with applications, First ed., McGraw-Hill, New York, 1995.

[14] D.W. Pepper, D. Carrington, Modeling Indoor Air Pollution, First ed., Imperial College Press, London, 2009.

[15] I. Salvado-Estivill, D.M. Hargreaves, G. Li Puma, Evaluation of the intrinsic photocatalytic oxidation kinetics of indoor air pollutants, Environ. Sci. Technol. 41 (2007) 2028-2035.

[16] A. Jarandehei, A. De Visscher, Three-dimensional CFD model for a flat plate photocatalytic reactor: Degradation of TCE in a serpentine flow field, AIChE Journal 55 (2009) 312-320.

[17] Z. Wang, J. Liu, Y. Dai, W. Dong, S. Zhang, J. Chen, CFD modeling of a UV-LED photocatalytic odor abatement process in a continuous reactor, J. Hazard. Mater. 215–216 (2012) 25-31.

[18] Y. Boyjoo, M. Ang, V. Pareek, Some aspects of photocatalytic reactor modeling using computational fluid dynamics, Chem. Eng. Sci. 101 (2013) 764-784.

[19] X. Wang, X. Tan, T. Yu, Kinetic study of ozone photocatalytic decomposition using a thin film of TiO2 coated on a glass plate and the CFD modeling approach, Ind. Eng. Chem. Res. 53 (2014) 7902-7909.

[20] S.R. Deng, S.W. Verbruggen, Z.B. He, D.J. Cott, P.M. Vereecken, J.A. Martens, S. Bals, S. Lenaerts, C. Detavernier, Atomic layer deposition-based synthesis of photoactive TiO2 nanoparticle chains by using carbon nanotubes as sacrificial templates, Rsc Adv. 4 (2014) 11648-11653.

[21] S.W. Verbruggen, S. Deng, M. Kurttepeli, D.J. Cott, P.M. Vereecken, S. Bals, J.A. Martens, C. Detavernier, S. Lenaerts, Photocatalytic acetaldehyde oxidation in air using spacious TiO2 films prepared by atomic layer deposition on supported carbonaceous sacrificial templates, Appl. Catal., B 160-161 (2014) 204-210.

[22] B. Hauchecorne, D. Terrens, S. Verbruggen, J.A. Martens, H. Van Langenhove, K. Demeestere, S. Lenaerts, Elucidating the photocatalytic degradation pathway of acetaldehyde: An FTIR in situ study under atmospheric conditions, Appl. Catal., B 106 (2011) 630-638.

[23] S.W. Verbruggen, J.J.J. Dirckx, J.A. Martens, S. Lenaerts, Surface photovoltage measurements: A quick assessment of the photocatalytic activity?, Catal. Today 209 (2013) 215-220.

[24] S.W. Verbruggen, K. Masschaele, E. Moortgat, T.E. Korany, B. Hauchecorne, J.A. Martens, S. Lenaerts, Factors driving the activity of commercial titanium dioxide powders towards gas phase photocatalytic oxidation of acetaldehyde, Catal. Sci. Technol. 2 (2012) 2311-2318.

[25] M.R. Hoffmann, S.T. Martin, W.Y. Choi, D.W. Bahnemann, Environmental Applications of Semiconductor Photocatalysis, Chem. Rev. 95 (1995) 69-96.

[26] L.L.P. Lim, R.J. Lynch, S.I. In, Comparison of simple and economical photocatalyst immobilisation procedures, Appl. Catal., A 365 (2009) 214-221.

[27] T.A. Egerton, C.J. King, Influence of Light-Intensity on Photoactivity in Tio2 Pigmented Systems, J. Oil Colour Chem. As. 62 (1979) 386-391.

[28] A.C. Cengel, A.J. Ghajar, Heat and Mass Transfer. Fundamentals and Applications, Fourth ed., McGraw-Hill, New York, 2011.

[29] S.B. Kim, S.C. Hong, Kinetic study for photocatalytic degradation of volatile organic compounds in air using thin film TiO2 photocatalyst, Appl. Catal., B 35 (2002) 305-315.

[30] Y. Xu, C.H. Langford, Variation of Langmuir adsorption constant determined for TiO2-photocatalyzed degradation of acetophenone under different light intensity, J. Photochem. Photobiol., A 133 (2000) 67-71.

[31] A. Mills, J. Wang, The Kinetics of Semiconductor Photocatalysis: Light Intensity Effects, Z. Phys. Chem. 213 (1999) 49-58.

418 Figure 1

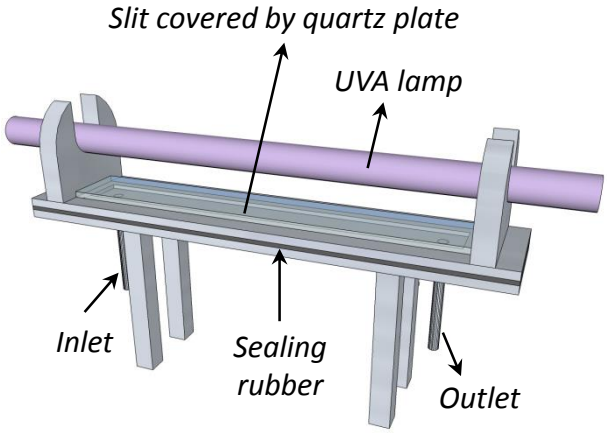


419

420

421 Figure 2

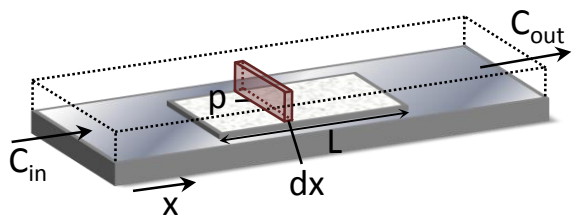


422

423

424 Figure 3

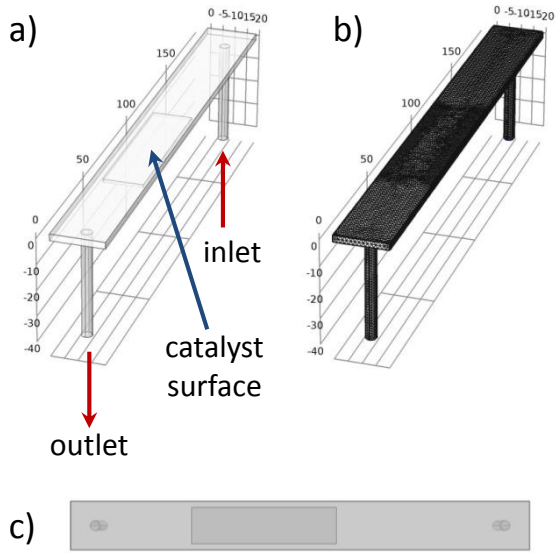


425

426

427 Figure 4

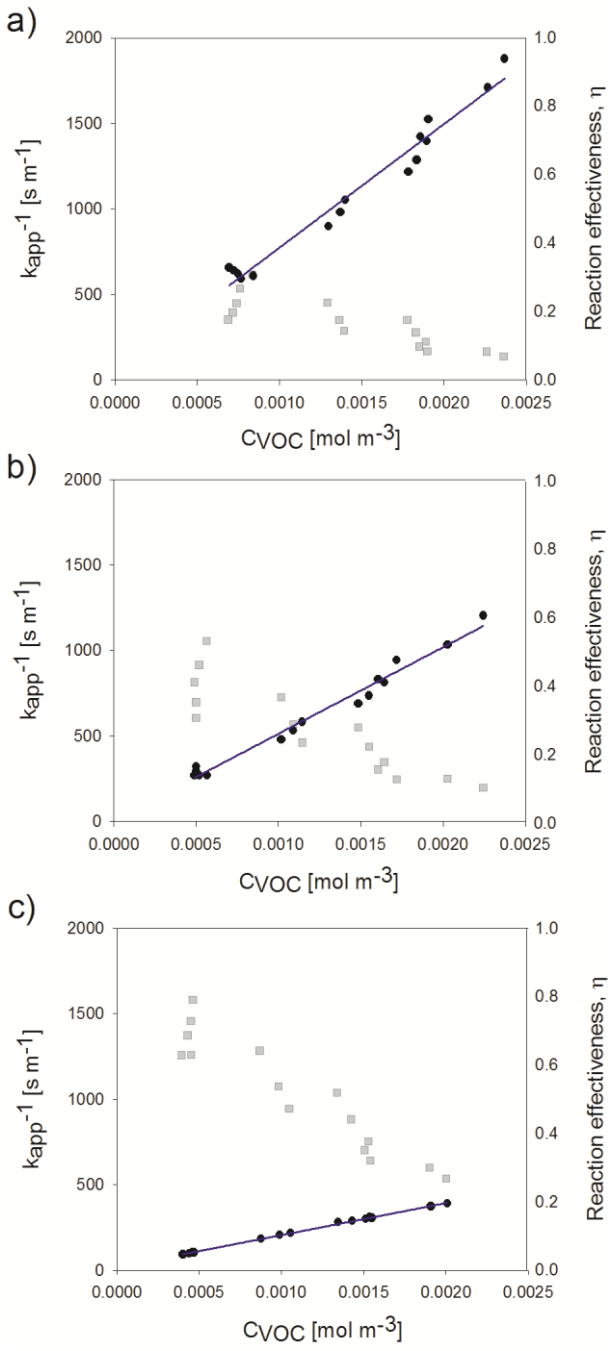


428

429

430 Figure 5

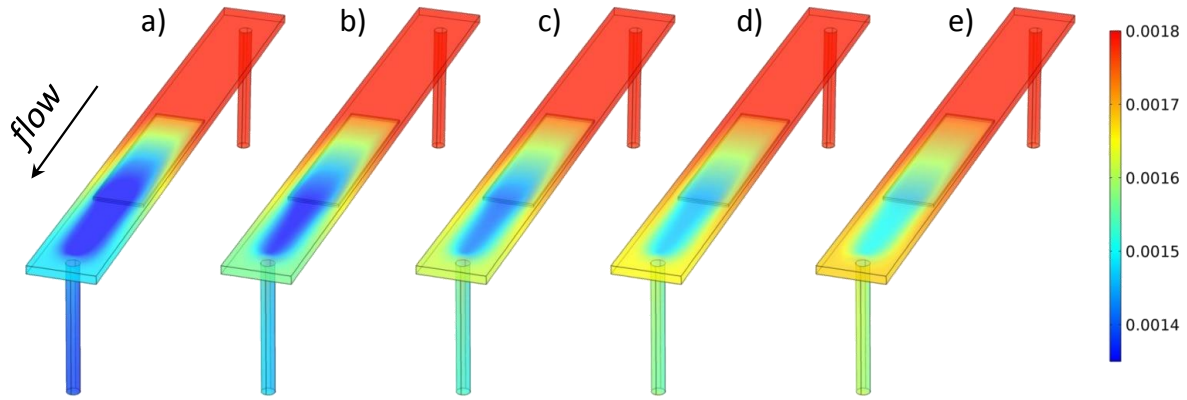


431

432

433 Figure 6

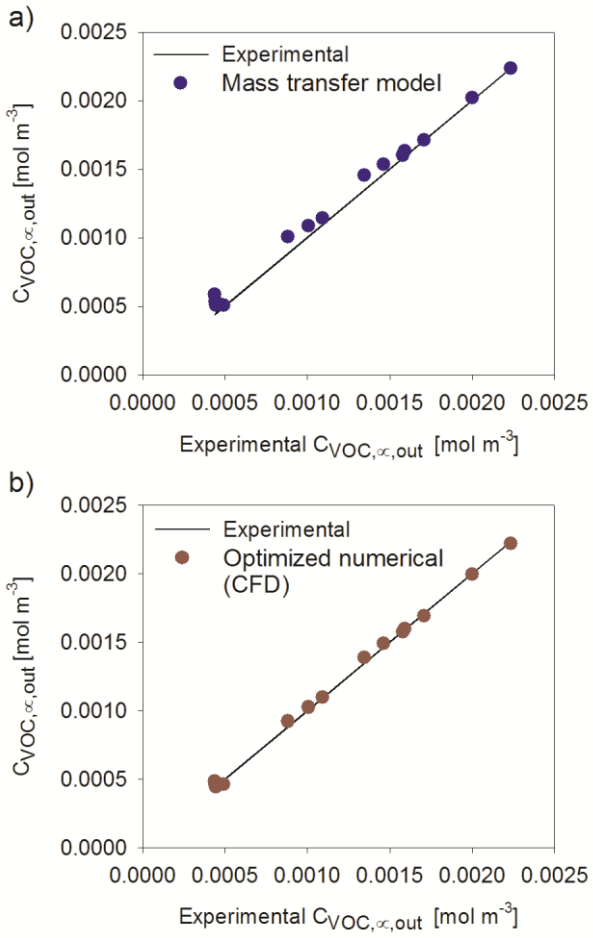


434

435

436 **Table 1.** General parameters on reactor geometry and fluid properties

| Parameter | Value |
|---|---|
| Slit height [m] | 0.0025 |
| Slit width [m] | 0.020 |
| Hydraulic diameter, $D_h$ [m] | 0.0044 |
| Catalyst layer width, $p$ [m] | 0.015 |
| Catalyst layer length, $L$ [m] | 0.06 |
| Catalyst layer surface, $A$ [$m^2$] | 0.0009 |
| Kinematic viscosity, $\nu$ [ $m^2 s^{-1}$] | $1.52 \times 10^{-5}$ |
| Acetaldehyde diffusion coefficient, $D$ [$m^2 s^{-1}$] | $1.24 \times 10^{-5}$ |
| Molecular weight [g $mol^{-1}$] | 44.05 |

437

438

439 **Table 2.** Experimental parameters of the mass transfer based model for the experiments at the intermediate UVA
440 illumination intensity of 1.8 mW $cm^{-2}$.

| Parameter | Total volumetric flow rate [$cm^3$ $min^{-1}$] | | | | |
|---|---|---|---|---|---|
| | 300 | 375 | 450 | 525 | 600 |
| Average flow velocity, $V_{avg}$ [m $s^{-1}$] | 0.1 | 0.125 | 0.15 | 0.175 | 0.2 |
| Reynolds number, *Re* | 29.3 | 36.6 | 44.0 | 51.3 | 58.6 |
| Sherwood number, *Sh* | 6.49 | 6.49 | 6.49 | 6.49 | 6.49 |
| Mass transfer coefficient, $h_{mass}$ [m $s^{-1}$] | 0.0181 | 0.0181 | 0.0181 | 0.0181 | 0.0181 |
| $NTU_{PCO,ideal}$ | 4.35 | 3.48 | 2.90 | 2.48 | 2.17 |
| $\varepsilon_{ideal}$ | 0.99 | 0.97 | 0.94 | 0.92 | 0.89 |
| | **ca. 22 ppmv inlet concentration** | | | | |
| Fractional conversion, $\varepsilon$ | 0.52 | 0.45 | 0.39 | 0.32 | 0.27 |
| Reaction effectiveness, $\eta$ | 0.53 | 0.46 | 0.41 | 0.35 | 0.31 |
| $NTU_{PCO}$ | 0.74 | 0.59 | 0.49 | 0.39 | 0.32 |
| Average total removing factor, $K_t$ | 0.0031 | 0.0031 | 0.0031 | 0.0029 | 0.0027 |
| Apparent rate constant, $k_{app}$ [m $s^{-1}$] | 0.0037 | 0.0037 | 0.0037 | 0.0034 | 0.0031 |
| | **ca. 43 ppmv inlet concentration** | | | | |
| Fractional conversion, $\varepsilon$ | 0.36 | 0.28 | 0.22 | 0.14 | 0.11 |
| Reaction effectiveness, $\eta$ | 0.37 | 0.29 | 0.24 | 0.16 | 0.13 |
| $NTU_{PCO}$ | 0.45 | 0.33 | 0.25 | 0.15 | 0.12 |
| Average total removing factor, $K_t$ | 0.0019 | 0.0017 | 0.0016 | 0.0011 | 0.0010 |
| Apparent rate constant, $k_{app}$ [m $s^{-1}$] | 0.0021 | 0.0019 | 0.0017 | 0.0012 | 0.0011 |
| | **ca. 53 ppmv inlet concentration** | | | | |
| Fractional conversion, $\varepsilon$ | 0.28 | 0.22 | 0.17 | 0.12 | 0.09 |
| Reaction effectiveness, $\eta$ | 0.28 | 0.22 | 0.18 | 0.13 | 0.10 |
| $NTU_{PCO}$ | 0.32 | 0.24 | 0.18 | 0.13 | 0.10 |
| Average total removing factor, $K_t$ | 0.0013 | 0.0013 | 0.0012 | 0.0009 | 0.0008 |
| Apparent rate constant, $k_{app}$ [m $s^{-1}$] | 0.0015 | 0.0014 | 0.0012 | 0.0010 | 0.0008 |

441

442

**Table 3.** Summary of the kinetic parameters calculated in accordance with the analytic mass transfer based method and the numeric method (CFD) after an optimization procedure.

| Intensity [mW $cm^{-2}$] | $k_{LH}$ [mol $s^{-1}$ $m^{-2}$] | | $K_L$ [$m^3$ $mol^{-1}$] | | *Overall reaction rate r [µmol $m^{-2}$ $s^{-1}$]** |
|---|---|---|---|---|---|
| | *Mass transfer based (analytic)* | *Optimized numeric (CFD)* | *Mass transfer based (analytic)* | *Optimized numeric (CFD)* | |
| 1.3 ± 0.1 | $1.38 \times 10^{-6}$ | $(1.58 \pm 0.13) \times 10^{-6}$ | $1.45 \times 10^{4}$ | $(1.78 \pm 0.15) \times 10^{4}$ | 1.31 ± 0.11 |
| 1.6 ± 0.1 | $2.11 \times 10^{-6}$ | $(2.40 \pm 0.20) \times 10^{-6}$ | $1.47 \times 10^{4}$ | $(1.65 \pm 0.11) \times 10^{4}$ | 1.94 ± 0.17 |
| 2.6 ± 0.1 | $5.35 \times 10^{-6}$ | $(6.23 \pm 0.47) \times 10^{-6}$ | $1.02 \times 10^{4}$ | $(1.16 \pm 0.08) \times 10^{4}$ | 4.79 ± 0.27 |

* calculated from (eq. 2) as the product of the apparent rate constant $k_{app}$ and $C_{VOC}$ (determined from the inlet and outlet bulk concentrations), averaged over all experiments at the given light intensity.

## Figure Captions

**Fig. 1:** Schematic representation of the flat bed reactor used in this work.

**Fig. 2:** Schematic representation of the reactor slit with the catalyst coated surface positioned in the center on the bottom reactor plate. The infinitesimal volume element is indicated in red. x is the coordinate of the flow direction. p is the length of the reaction surface perpendicular to the direction of flow.

**Fig. 3.** Illustration of a) the reactor geometry and b) the computational grid (mesh) for the plate reactor, overall view and c) top view.

**Fig. 4.** Plot of $k_{app}^{-1}$ (●)and $\eta$ (□) *versus* the average surface concentration $C_{VOC}$ for a) (1.3 ± 0.1) mW $cm^{-2}$, b) (1.8 ± 0.1) mW $cm^{-2}$ and c) (2.6 ± 0.1) mW $cm^{-2}$ incident UVA intensity.

**Fig. 5.** Distributions of acetaldehyde concentrations calculated using CFD simulations in steady state condition. The acetaldehyde inlet concentration was 43 ppmv (0.00179 mol $m^{-3}$), at an effective total inlet gas flow rate of: a) 300 $cm^3$ $min^{-1}$, b) 375 $cm^3$ $min^{-1}$, c) 450 $cm^3$ $min^{-1}$, d) 525 $cm^3$ $min^{-1}$ and e) 600 $cm^3$ $min^{-1}$.

**Fig. 6.** Comparison of the calculated outlet VOC concentrations (data points) with the experimentally determined outlet VOC concentrations (black straight line) using a) the kinetic parameters determined by the analytic mass transfer based model and b) the numeric method (CFD).